Journal of Biomedical Optics

SPIEDigitalLibrary.org/jbo

Enhanced laser tissue soldering using indocyanine green chromophore and gold nanoshells combination

Mohammad E. Khosroshahi
Mohammad S. Nourbakhsh

SPIE

Enhanced laser tissue soldering using indocyanine green chromophore and gold nanoshells combination

Mohammad E. Khosroshahi[a] and Mohammad S. Nourbakhsh[b]
[a]Amirkabir University of Technology, Faculty of Biomedical Engineering, Biomaterial Group, Laser and Nanobiophotonics Laboratory, Tehran-Iran
[b]Semnan University, Department of Engineering, Material Science and Engineering Group, Semnan, Iran

Abstract. Gold nanoshells (GNs) are new materials that have an optical response dictated by the plasmon resonance. The wavelength at which the resonance occurs depends on the core and shell sizes. The purposes of this study were to use the combination of indocyanine green (ICG) and different concentration of gold nanoshells for skin tissue soldering and also to examine the effect of laser soldering parameters on the properties of repaired skin. Two mixtures of albumin solder and different combinations of ICG and gold nanoshells were prepared. A full thickness incision of 2×20 mm^2 was made on the surface and after addition of mixtures it was irradiated by an 810 nm diode laser at different power densities. The changes of tensile strength (σ_t) due to temperature rise, number of scan (Ns), and scan velocity (Vs) were investigated. The results showed at constant laser power density (I), σ_t of repaired incisions increases by increasing the concentration of gold nanoshells in solder, Ns, and decreasing Vs. It was demonstrated that laser soldering using combination of ICG + GNs could be practical provided the optothermal properties of the tissue are carefully optimized. Also, the tensile strength of soldered skin is higher than skins that soldered with only ICG or GNs. In our case, this corresponds to $\sigma_t = 1800$ g cm^{-2} at $I \sim 47$ Wcm^{-2}, $T \sim 85\,^{o}$C, $Ns = 10$, and $Vs = 0.3$ mms^{-1}.
[DOI: 10.1117/1.3611001]

Keywords: tissue soldering; diode laser; indocyanine green + gold nanoshells; tensile strength.

Paper 10517RRR received Sep. 29, 2010; revised manuscript received Jun. 12, 2011; accepted for publication Jun. 22, 2011; published online Aug. 9, 2011.

1 Introduction

Basically there are two distinct approaches to laser tissue bonding: 1. laser tissue welding (LTW), in which laser energy is applied to the well-approximated edges of a tissue; and 2. laser tissue soldering (LTS), in which various substances (as solders) are applied on the approximated edges of the tissue, before the lasing process. The application of laser welding was limited by the large zone of thermal damage produced, low-bond strength, and inconsistency of results.[1,2] One of the pioneering works on the effect of laser irradiation on tensile strength and surgical wound healing was done by Braverman and his co-workers.[3] Also, the kinetics of a tissue fusion process (laser welding) was studied by Pearce et al.[4] Their models estimate collagen damage based on kinetics thermal damage analysis and water loss boundaries as a function of irradiation beam parameters and heating time.

The application of a protein solder to the tissue being welded promises to overcome this problem, as it provides additional protein to strengthen the bond, while not triggering the foreign body reaction. To enhance the laser light absorption, a suitable dye may be added to the protein solder.[5–7] This localizes the heat generated by the laser light to the region of the protein glue, protecting the underlying tissue from excessive heat. Another advantage of using a chromophore is the use of available semiconductor diode lasers with wavelengths close to their absorption peak.[8–10]

Recent attempts with other solder and laser combination have utilized thermal cameras and thermocouples in order to detect potentially high tissue temperatures during the laser process.[11,12] These feedback systems usually consist of some sensors that measure the tissue parameters of interest, coupled to a feedback loop that adjust the laser power density in response to the measurements.[13,14] LTS has been successfully utilized in anastomoses of various tissues including the blood vessels,[15–17] cartilage[18] and skin.[19–21]

The conduction band electrons in metals can undergo a coherent oscillation, the so-called plasma oscillation. The electromagnetic field of the incoming light wave can induce polarization of the conduction electron, which means the electrons are displaced with respect to the heavier positive core ions. The dielectric response of a metal to electromagnetic radiation is given by the complex dielectric constant

$$k_{sp} = \frac{\omega}{c}\sqrt{\frac{\varepsilon_c \varepsilon_m}{\varepsilon_c + \varepsilon_m}}, \quad (1)$$

where k_{sp} is the surface plasmon wave vector, ω is the frequency of light, and ε_c, ε_m represent the dielectric of core (SiO_2) and Au, respectively. It should be noted that ε_c is the (purely real) dielectric constant, and $\varepsilon_m = \varepsilon_r + J\varepsilon_i$ is the complex dielectric constant of the metallic nanoparticles. The real part (ε_r) determines the degree to which the metal polarizes in response to an applied external electric field and the imaginary part, $j\varepsilon_i$, quantifies the relative phase shift of this induced polarization with respect to the external field and it includes losses (e.g., ohmic

Address all correspondence to: Mohammad E. Khosroshahi, Amirkabir University of Technology, Faculty of Biomedical Engineering, Biomaterial Group, Laser and Nanobiophotonics Laboratory, Hafez Tehran, Tehran 15875-4413 Iran; Tel: +9821645542398; Fax: +982166468186; E-mail: khosro@aut.ac.ir.

1083-3668/2011/16(8)/088002/7/$25.00 © 2011 SPIE

loss as heat). The interaction of light and nanoparticles affects the displacement of charges, which in turn affects the coupling strength. Such nanoparticles exhibit strong optical scattering and absorption at the above region due to localized surface plasmon resonance (LSPR). This is a classical effect in which the light's electromagnetic field drives the collective oscillation of the nanoparticles free electrons into resonance. The resonance is the effect of maximum oscillation amplitude at particular frequency.[22–24] Gold nanoshells are the type of nanoparticles composed of normally silica cores coated with an ultrathin gold layer. They are biologically inert and optically tunable.[25,26] The optical properties can be tuned by varying the relative size of the core and the thickness of the shell. In particular, these particles can be designed to absorb near infrared light, and when irradiated by a laser, provide an exogenous vehicle to convert optical energy into heat. The interest lies in the unusually large absorption cross sections, which are much larger than geometric cross sections, at wavelengths corresponding to surface modes in the particle.[27] A variety of therapeutic applications for this phenomenon are being explored that exploit the temperature change induced by the strong plasmon-induced surface heat flux of nanoshells.[28,29]

Nanoshells have a number of advantages compared with ICG chromophore such as reduced diffusion from the site of treatment for sizes of about 100 nm and heat accumulation at the soldering interface. This in effect can help to reduce undesirable thermal damage to the surrounding healthy tissue.[30] Another advantage is their photo stability due to absorption properties and that they are not so sensitive to photo bleaching like ICG when exposed to light.[31,32] Moreover, nanoshells are stronger absorbers and, according to Lia et al.,[33] the absorption cross section of ICG is in the order of 10^{-20} m^2 and that for nanoshells is about 10^{-14} m^2, which implies they are almost one-million fold more effective absorbers.

In the previous works, we used an 810-nm diode laser with bovine serum albumin (BSA) as a biological solder containing ICG (Ref. 19) and gold nanoshells[34] as absorbing chromophore for skin tissue soldering. The purpose of this study was to evaluate and report the laser parameters necessary for effective LTS with ICG + GNs as an exogenous absorber at a different concentration.

2 Material and Methods

2.1 *Gold Nanoshell Synthesis and Characterization*

Synthesis of gold nanoshells was previously described in literature.[34] The UV/visible spectra of the nanoparticles were measured in solution using the spectrophotometer (Philips PU 8620) in the wavelength range of 190 to 900 nm. The morphology and dimensions of the nanoshells were analyzed using transmission electron microscopy (TEM) (Phillips CM-200-FEG) operating at 120 kV. The surface topography and roughness as well as the size of nanoshells were studied by atomic force microscopy (AFM) (Dual scope/ Raster scope C26, DME, Denmark).

2.2 *Preparation of Protein Solders Solutions*

Protein solder solution was prepared by dissolving 25% per weight BSA (Sigma Chemical Co.) and combination of 0.25 mg/ml ICG dye (Sigma Chemical Co.) and 1 and 2 ml of gold nanoshell suspension mixed in 5 ml high-performance liquid chromatography (HPLC) grade water. Thus, the protein solder consisted of 7×10^{10} nanoparticles/ml.

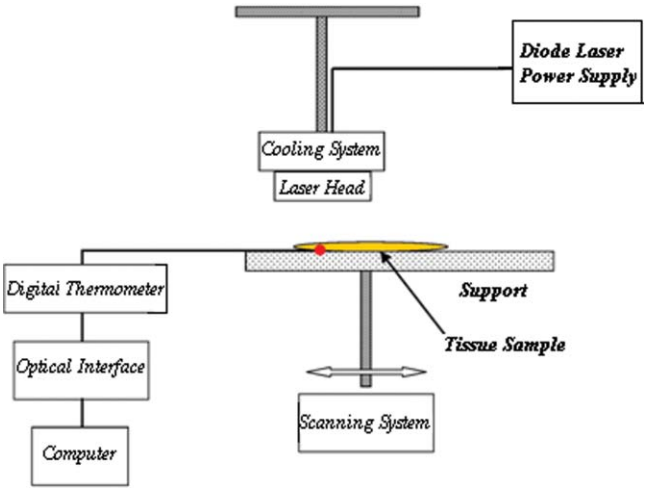

Fig. 1 Experimental setup for *in vitro* laser soldering of skin. The system includes a 810-nm diode laser, a scanning system, a digital thermometer, and a computer.

2.3 *In vitro Skin Soldering*

A 40 cm × 50 cm fresh piece of sheep skin was obtained from a slaughter house and was suitably depilated and cut into strips of 4 cm × 5 cm. The thickness of the skin samples was measured and found to be ~2 mm. The prepared samples were stored in a refrigerator at 4 °C for a maximum of 3 h. After preparation, a full thickness cut, 2 mm thick and 20 mm long, was made on the skin surface using 11-inch blades and soldered afterward.

The set-up of the used laser soldering system is shown in Fig. 1.[34] The system includes the following components: 1. a tunable continuous wave (CW) 1.5–6 W diode laser with a peak emission wavelength of 810 ± 20 nm and a rectangular beam profile of 1 mm × 7 mm connected to a cooling head, 2. an automatic programmable scanning system that moves the skin sample beneath the laser head, 3. a digital K-type thermometer (CHY502A1, CHY Firemate Co., Taiwan) with a probe diameter of 0.5 mm and a response time of 0.1 s that was positioned directly under the skin strips as illustrated in Fig. 1. However, it must be noted one of major limitations of such thermocouple is its delayed response time (100 milliseconds) which means no information about tissue temperature rise is achieved at earlier stage of irradiation. This component moved with the skin and measured the skin temperature during laser soldering, 4. an RS-232 optical interface connecting the thermometer to the computer and 5. a computer for recording and analyzing the thermometer signals.

For each concentration of nanoshells, 50 μl of the protein solder solution was applied to the cut edges and the edges were brought into contact with one another and then irradiated with different power densities (24 to 83 W/cm^2). In this procedure, the laser head was located at a distance of 8 mm perpendicular to the skin samples, and the scanning system was moved at a predefined speed varying between 0.2 and 0.42 mm/s until the

soldering process was completed. In addition, the effect of the number of scans on the tensile strength of the repaired skin was studied for each solder combination.

The temperature rise on the skin during the irradiation process was measured using a digital thermometer. The laser beam moved from one position to the next in a continuous mode along the cut line in such a way that the treated zones slightly overlapped so that no area was left untreated. Tensile strength measurements were performed within 30 min after the completion of the laser soldering process to test the integrity of the resultant repairs using a load machine (HCT 25/400 series, Zwick/Roell, Germany). Skin strips were inserted into the head of the loading machine, and tensile strength measurements were carried out with a constant crosshead return speed of 2 mm/min. An automatic data acquisition system was used to collect the data during the tensile test. The tensile strength was calculated by dividing the maximum load at the rupture point (F) by the cross-sectional area of the specimen. For each solder combination and laser parameter the experiment was repeated five times. For basic histological examination the skin specimen were sectioned perpendicular to the cut and then fixed in a 4% formaldehyde solution and transferred to baths of concentrated ethanol to remove the water. This step was followed by alcohol removal using a hydrophobic clearing agent (such as xylene), at which point the samples were embedded in paraffin. Finally, the specimens were cut into 4-μm slices and stained with haematoxylin eosin (H&E).

For comparison of results, the p-values for the differences between different combinations for each of the laser soldering parameters (power density, number of scan and scan velocity) were calculated using a one-way analysis of variance (ANOVA). Each final data represents an average of five readings. Statistically significant differences were considered at p-values < 0.05 (i.e., a significance level of 5%).

3 Results

UV-visible spectrum recorded for gold nanoshells is shown in Fig. 2. The resonance peak position depends on the plasmon interaction between separate inner and outer gold layers. The optical absorption spectra shown in Fig. 2 are relatively broad compared with that of pure gold colloid. According to the Mie scattering theory, the nanoshells geometry can quantitatively accounts for the observed plasmon resonance shifts and line-widths. In addition, the plasmon line-width is dominated by surface electron scattering.

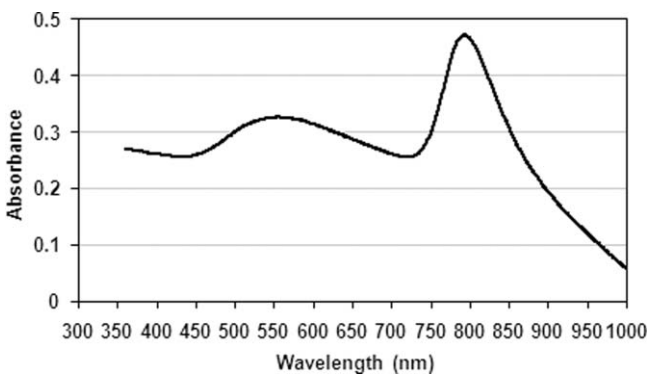

Fig. 2 UV-visible spectrum of gold nanoshells.

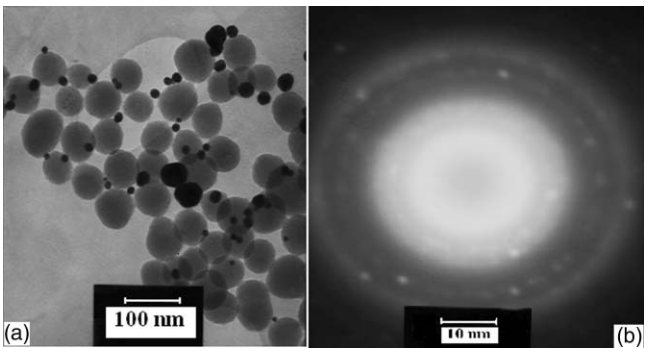

Fig. 3 (a) TEM photographs and (b) SAED pattern of gold nanoshells formation.

A TEM (PHILIPS CM120) image of the gold nanoshell is shown in Fig. 3(a) and a selected area electron diffraction pattern of gold nanoparticles is shown in Fig. 3(b), which illustrates the crystalline nature of gold particle. An example of Au-coated SiO_2 nanoshells and their three-dimensional images taken by AFM are shown in Figs. 4(a) and 4(b), respectively.[34]

The tensile strength (σ) of the repaired specimens determined from the mean of five cuts was measured as a function of laser power density and solders combination and is shown in Fig. 5. As shown in Fig. 5, the value of σ_t increased with increasing power density and nanoshell concentration in the solder. However, for the latter case, the difference is not statistically significant.

An example of the thermal signal received from the skin surface during the laser soldering process with $I = 60$ W/cm^2 is shown in Fig. 6(a), where each peak was observed when the laser beam was coincident with the tip of the thermometer. The variation in the tissue temperature (T) with laser power density for different solder combination is shown in Fig. 6(b).

The effect of the number of scans (Ns) on the tensile strength of the repaired skin for two different solder combinations at a constant power density is illustrated in Fig. 7. For a given constant power density the tensile strength increased with the increasing number of scans. This may be explained by the fact that a higher number of scans cause a greater temperature rise, and hence, more thermal denaturation occurs. Moreover, overlap between sections of a region that was heated during the first round and the heat produced during the second scan can enhance this effect. Figure 8 indicates that, at a constant I, an increase in

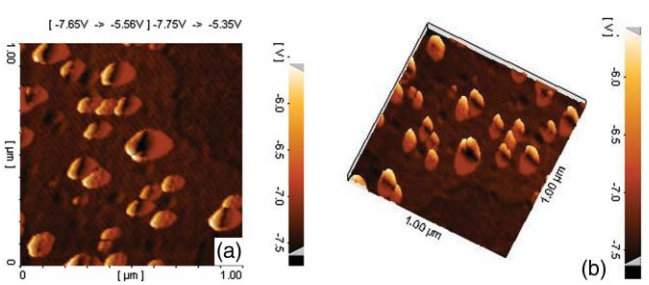

Fig. 4 AFM photographs of surface topography of SiO_2/Au nanoshells (a) two dimensional and (b) three dimensional.

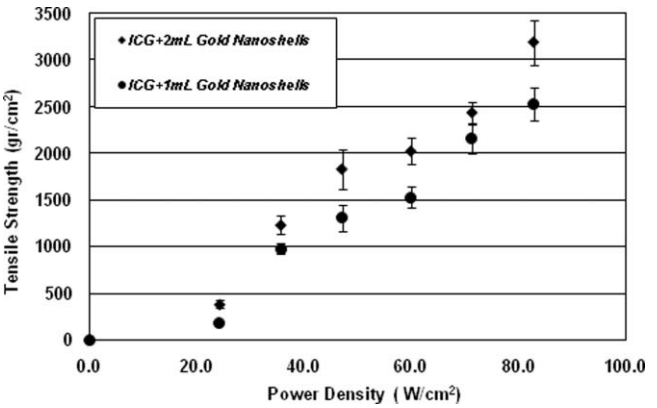

Fig. 5 Variation of tissue tensile strength with laser power density at constant solder combination.

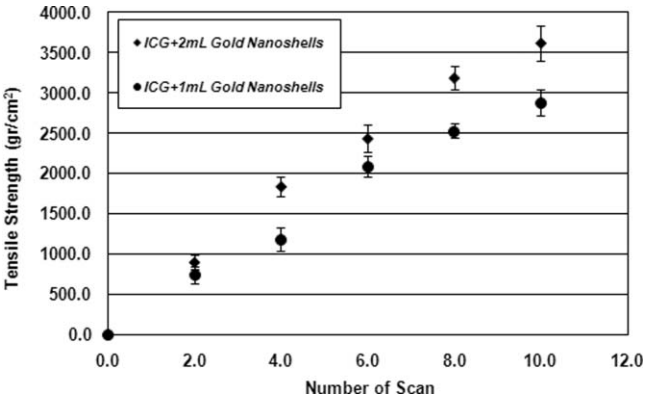

Fig. 7 Effect of number of laser scans and solder combination on tissue tensile strength at a given power density.

the scan velocity cause the corresponding value of σ to decrease due to a smaller temperature rise.

Histological images of laser soldered incisions by 47 Wcm^{-2} and is illustrated in Figs. 9(a) and 9(b). A very mild burn was observed on the right margin of the bonded wound, represented by a basophilic stain (H&E, original magnification × 10).

4 Discussions

In the current study, we have reported the use of combination of ICG and SiO_2/Au nanoshells (ICG + GNs), as an exogenous near infrared absorber and focused on the laser parameters necessary for effective LTS with different concentration of nanoshells. The nanoshells used in these experiments had a diameter of ∼110 nm and a shell thickness of ∼10 nm. As seen in Fig. 2, the absorption peak of gold nanoshells is ∼795 nm and that for ICG is ∼800 nm both of which are close to the wavelength of the diode laser (810 nm).

Of course, there always will be some colloidal contamination in synthesis process. However, in our case since the maximum absorption peak is at ∼800 nm, it indicates the majority of the nanoparticles are gold nanoshells and not just gold colloid (i.e., the second peak at ∼550 nm). Also, the presence of ICG with maximum absorption peak at ∼810 nm would help to reduce or even prevent from further effect of contamination on the results.

Hence, in principal the combination of gold nanoshells and ICG can be suitable for LTS using a diode laser. Nanoshells are also intense absorbers. Conventional NIR dyes like ICG possess an absorption cross section of 2.9×10^{-20} m^2 at 800 nm. In contrast, according to Mie scattering theory that predicts the metal nanoshells possess an absorption cross section on the order of 3.8×10^{-14} m^2, which is greater by a factor of 106 compared to that of ICG. However, it is clearly demonstrated that gold nanoshells display much stronger absorptive compared with ICG molecules.[35]

In the current study, we have used the combination of ICG and gold nanoshells, as exogenous near infrared absorbers for enhancement of selective photo thermal interaction on thermal

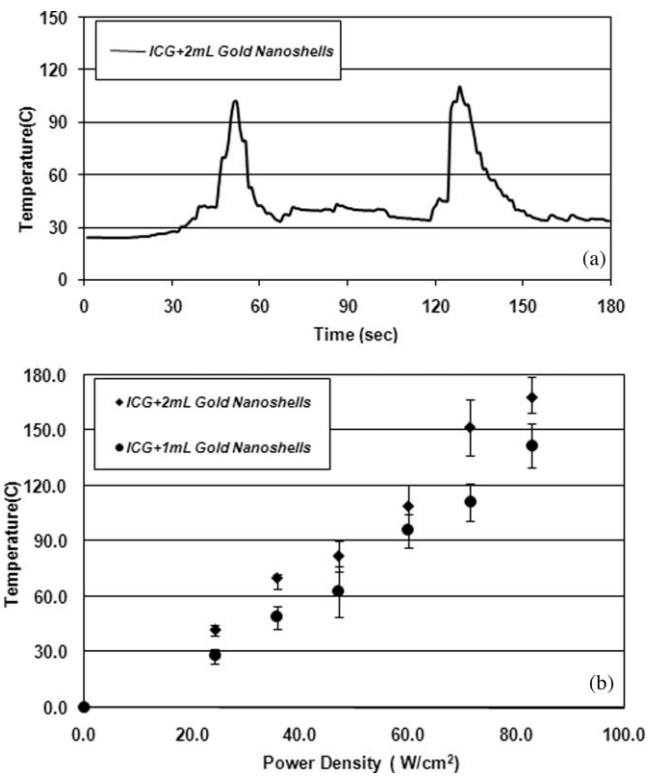

Fig. 6 Tissue temperature rise (a) as a function of time where two consecutives peaks represents a complete round trip at 60 W cm^{-2} and (b) as a function of laser power density.

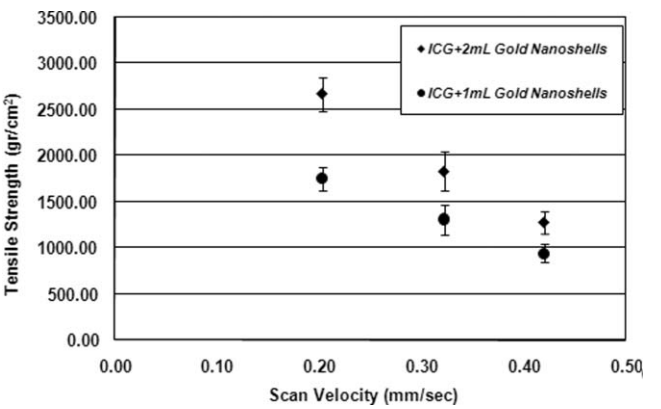

Fig. 8 Effect of laser scans velocity on tissue tensile strength at a given power density.

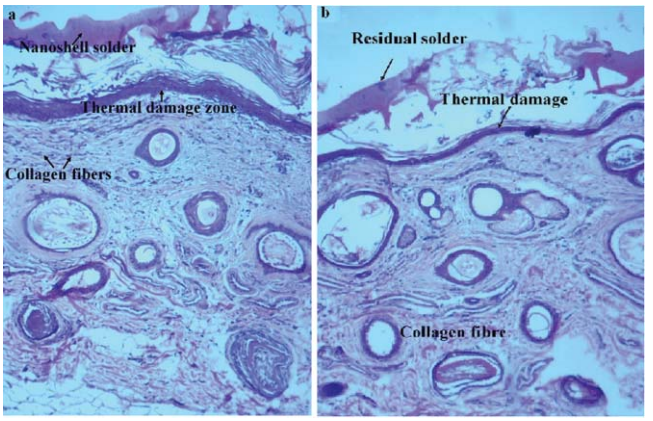

Fig. 9 (a) and (b) Histological images of laser soldered incisions at 47 W cm^{-2}.

and biomechanical properties of skin tissue and LTS. The nanoshells used in our experiments had an average diameter of ~100 nm (85 to 115 nm) and a shell thickness of ~10 nm (7 to 12 nm) measured by TEM.

The optical properties of nanoshells are well predicted by Mie scattering theory,[36,37] thus allowing one to calculate the dimensions of core and shell required to fabricate nanoshells with strong absorption at a given wavelength. This allows facile tuning to match the output of a desired laser source for a given application. Extinction cross section includes both absorption and scattering

$$C_{ext} = C_{Sca} + C_{abs}. \tag{2}$$

The extinction cross section for a small core-shell particle is

$$C_{ext} = k\ Im\ (\alpha), \tag{3}$$

where $k = 2\pi\sqrt{\varepsilon_m}/\lambda$, λ is the wavelength of the incident light in vacuum and Im (α) is the imaginary part of complex polarizability of the particle

$$a = \varepsilon_0 \frac{(\varepsilon_s - \varepsilon_m)(\varepsilon_c + 2\varepsilon_s) + (R_c/R_s)^3(\varepsilon_c - \varepsilon_s)(\varepsilon_m + 2\varepsilon_s)}{(\varepsilon_s + 2\varepsilon_m)(\varepsilon_c + 2\varepsilon_s) + (R_c/R_s)^3(\varepsilon_c - \varepsilon_s)(2\varepsilon_s - \varepsilon_m)} 4\pi R_s^3. \tag{4}$$

$\varepsilon_0 = 8.85\times10^{-12} F/m$ is the permittivity of free space, R_c is the radius of core, R_s is the total particle size including shell thickness, and ε_c, ε_s, and ε_m are the dielectric function of core, shell, and embedding media, respectively.

Laser-bonding was proposed as a preferred method for sealing wounds, which include tissue incisions in general and skin incisions in particular.[19,38] The rationale behind the tissue laser-bonding procedure is that this technological platform may offer minimal inflammation traits with only minimal scar formation.[39,40] Laser-soldering temperatures below 60 °C generated a weak bond,[24] while laser soldering at temperatures exceeding 80 °C induced thermal damage. Since one of the objectives of this work was to select an optimal temperature setting that will not induce thermal damage, therefore, the optimal temperature for soldering was 65 °C. As it is shown in Fig. 6, the temperature rise of skin increases with increasing laser power density and the concentration of gold nanoshell in dye combination. For power density above 47 Wcm^{-2}, the temperature exceeds 90 °C and it is not suitable for *in vivo* application. In comparison with our previous results with gold nanoshells alone, this condition occurs above 60 Wcm^{-2},[34] so we can conclude that by adding of ICG in albumin solder one may use lower power densities for LTS with acceptable results. Varying the power density on ICG + GNs solder resulted in a slight rise of temperature and tensile strength, it may be, however suggested that Ns and, hence, scan velocity (Vs) significantly affect the σ as well as the quality of soldered tissue. This can be argued by the fact that while Vs controls the temperature rise for intertwining tissue fibrillar collagen matrix and subsequent melting transition and fusion, Ns influences the thermal accumulation effect on the tissue.

Our results indicate that laser power density is the most important parameter affecting solder temperature during the process of laser tissue soldering. Also, varying the gold nanoshells concentration within the solder resulted in similar thermal behavior with insignificant changes of temperature. The findings of this study show that temperatures recorded beneath the skin can reach up to 80 °C or even higher considering the thermocouple limitation. However, it is important to notice that the thermocouple properties can directly affect the temperature measurements. As was shown by Verdaasdonk et al.[41] that tissue temperature rise can be mainly influenced by number of parameters, direct absorption of radiation by probe, and also by their geometry. Also, a thermal gradient was observed both laterally and in front of the probe. On the other hand, the limitations of such digital thermometer including the size or diameter of thermocouple head as well as its position relative to the center of exposure should be taken into account. Therefore, we believe for a more accurate conclusion, the above issues must be considered. Needless to say, the use of a digital thermal camera for such investigations seems to be more appropriate as it will be used in our further research.

Increasing tensile strength with power density has the same trend in comparison with nanoshells and ICG alone, but in each power density the tensile strength in the case of ICG + GNs is higher. For example, the tensile strengths of repaired skin at a power density of 47 Wcm^{-2} are 1190 ± 90, 1422 ± 120, and 1830 ± 215 g cm^{-2} for ICG, gold nanoshells, and ICG + GNs, respectively. Studies by DeCoste et al.[42] using ICG dye alone showed that at temperatures above 60 °C a significant release of ICG and a steep increase in the temperature. This presumably resulted from the release of ICG from collagen as the molecule reached its fibrillar melting transition temperature. In a study by Kirsch et al.[43] temperatures during laser activation with an ICG/albumin solder were determined within the solder and underlying dermis over one minute of activation. Their results showed that the temperature within the solder reached 101 °C, while temperature in the superficial and deep skin was 70 and 65 °C, respectively. The results of Fung et al.[44] showed that wounds repaired at higher temperatures (85 and 95 °C) were observed to have lower mean wound strength than wounds repaired at lower temperatures (65 and 75 °C).

The effect of number of scan on tensile strength of repaired skin is also studied. At eight scans and power density of 83 Wcm^{-2}, the tensile strength of soldered skin with ICG alone is 1920 ± 80 g cm^{-2}, which at the same condition this value is 2407 ± 124 and 3189 ± 139 g cm^{-2} for gold nanoshells and combination of ICG and gold nanoshells, respectively. Also, with a combination of these light absorbers we can achieve the acceptable tensile strength in comparison with previous studies

Table 1 Comparison of tensile strengths (σ_t) results with different solder and laser parameters. Column 1 from Ref. 19 and column 2 from Ref. 34. The data is in units of g cm^{-2}.

	Solder		
Laser Parameters	LTS: ICG	LTS: Gold nanoshell	LTS: ICG + GNs
I (47 Wcm^{-2})	1075 ± 90	1422 ± 120	1830 ± 210
I (60 Wcm^{-2})	1400 ± 120	1610 ± 110	2022 ± 140
I (83 Wcm^{-2})	1920 ± 110	2407 ± 162	3189 ± 240
$Ns = 4$	630 ± 80	930 ± 80	1180 ± 122
$Ns = 8$	1300 ± 75	1860 ± 95	2530 ± 90
$Vs = 0.2$ mms^{-2}	1800 ± 140	2120 ± 90	2670 ± 180
$Vs = 0.3$ mms^{-2}	1350 ± 190	1422 ± 160	1830 ± 210
$Vs = 0.4$ mms^{-2}	1080 ± 90	1200 ± 125	1280 ± 210

with a lower number of scans. For example, using four scans, the tensile strength reached 1840 ± 122 g cm^{-2}, which is comparable to tensile strength of soldered skin with ICG using eight scans. This finding can be important for clinical applications if less operation time is considered.

As shown in Fig. 8, by decreasing the scan velocity, the tensile strength of repaired skin increased for different concentrations of gold nanoshells in combination of solder. For a constant scan velocity, for example 0.3 mms^{-1}, tensile strength of skin soldered with ICG, gold nanoshells, and a combination of ICG and gold nanoshells was 1350 ± 120, 1422 ± 160, and 1830 ± 210 g cm^{-2}, respectively. The latter value is the same as the tensile strength achieved by Vs of 0.2 mms^{-1} for ICG alone. The comparison of the tensile strengths results (σ_t) achieved by different solders and laser parameters is given in Table 1.

5 Conclusions

We have demonstrated that a combination of gold nanoshells and ICG can produce a better exogenous absorber and, hence, a more reliable result for tissue soldering. The results showed that the tensile strength of the repaired skin increases with increasing power density for both concentrations of solder. But the concentration of gold nanoshells does not seem to significantly affect the tensile strength. By increasing the scan velocity, the tensile strength of repair and operation time decreases, which should be taken into account in any operation. Thus, it can tentatively be concluded that since the skin temperature should not exceed ~90 °C at any time of work,[45] then the acceptable conditions in our experiment correspond to $\sigma_t = 1800$ g cm^{-2} at $I \sim 47$ Wcm^{-2}, $T \sim 85$ °C, $Ns = 10$, and $Vs = 0.3$ mms^{-1}.

References

1. R. B. Stewart, C. B. Bleustein, P. B. Petratos, K. C. Chin, D. P. Poppas, and R. T. Kung, "Concentrated autologous plasma protein: a biochemically neutral solder for tissue welding," *Lasers Surg. Med.* **29**, 336–342 (2001).
2. A. Lauto, J. Foster, L. Ferris, A. Avolio, N. Zwaneveld, and L. P. Warren, "Albumin–genipin solder for laser tissue welding," *Lasers Surg. Med.* **35**(2), 140–145 (2004).
3. B. Braverman, R. J. McCarthy, A. D. Ivankovich, D. E. Forde, M. Overfield, and M. S. Bapna, "Effect of helium- neon and infrared laser irradiation on wound healing in rabbits," *Lasers Surg. Med.* **9**, 50–58 (1989).
4. J. A. Pearce and S. Thomsen, "Kinetic models of tissue fusion," *Proc. of Laser Surgery (SPIE): Advanced Characterization, Therapeutics, and Systems III* **1643**, 251–260 (1992).
5. M. C. Oz, J. P. Johnson, S. Parangi, R. S. Chuck, C. C. Marboe, L. S. Bass, R. Nowygrod, and M. R. Treat, "Tissue soldering by use of indocyanine green dye-enhanced fibrinogen with the near infrared diode laser," *J. Vasc. Surg.* **11**, 718–725 (1990).
6. L. S. Bass, "Laser tissue welding: a comprehensive review of current and future clinical applications," *Lasers Surg. Med.* **17**, 315–349 (1995).
7. M. Gulsoy, Z. Dereli, and H. Tabakogh, "Closure of skin incisions by 980 nm diode laser welding," *Lasers Med. Sci.* **2**, 5–10 (2006).
8. A. Capon, E. Souil, B. Gauthier, C. Sumian, M. Bachelet, B. Buys, B. S. Polla, and S. Mordon, "Laser assisted skin closure (LASC) by using a 815 nm diode laser system accelerates and improves wound healing," *Lasers Surg. Med.* **28**(2), 168–175 (2001).
9. C. S. Cooper, I. P. Schwartz, D. Suh, and A. J. Kirsch, "Optimal solder and power density for diode laser tissue soldering (LTS)," *Lasers Surg. Med.* **29**(1), 53–61 (2001).
10. K. M. McNally, B. S. Sorg, and A. J. Welch, "Novel solid protein solder designs for laser-assisted tissue repair," *Lasers. Surg. Med.* **27**(2), 147–157 (2000).
11. D. Simhon, A. Ravid, M. Halpern, I. Cilesiz, T. Brosh, and N. Kariv, "Laser soldering of rat skin, using fiberoptic temperature controlled system," *Lasers Surg. Med.* **29**, 265–273 (2001).
12. D. Spector, Y. Rabi, I. Vasserman, A. Hardy, J. Klausner, and A. Katzir, "In vitro large diameter bowel anastomosis using a temperature controlled laser tissue soldering system and albumin stent," *Lasers Surg. Med.* **41**, 504–508 (2009).
13. L. I. Deckelbaum, S. P. Desai, K. Chang, and J. J. Scott, "Evaluation of a fluorescence feedback system for guidance jn laser angioplasty," *Lasers Surg. Med.* **16**, 226–234 (1995).
14. D. P. Poppas, R. B. Stewart, J. M. Massicotte, A. E. Wolga, R. T. Kung, A. B. Retik, and M. Freeman, "Temperature–controlled laser photocoagulation of soft tissue: in vivo evaluation using a tissue welding model," *Lasers Surg. Med.* **18**, 335–344 (1996).
15. A. C. O'Neill, J. M. Winograd, J. L. Zeballos, M. A. Randolph, K. E. Bujold, I. E. Kochevar, and R. W. Redmond, "Microvascular anastomosis using a photochemical tissue bonding technique," *Lasers Surg. Med.* **39**, 716–722 (2007).
16. H. Xie, S. C. Bendre, A. P. Burke, K. W. Gregory, and A. P. Furnary, "Laser-assisted vascular end to end anastomosis of elastin heterograft to carotid artery with an albumin stent: A preliminary in vivo study," *Lasers Surg. Med.* **35**, 201–205 (2004).
17. B. S. Sorg, K. M. Mcally, and A. J. Welch, "Biodegradable polymer film reinforcement of a indocyanine green-doped liquid albumin solder for laser-assisted incision closure," *Lasers Surg. Med.* **27**, 73–81 (2000).
18. B. Zuger, B. Ott, T. Schaffner, and J. Clemence, "Laser solder welding of articular cartilage: Tensile strength and chondrocyte viability," *Lasers Surg. Med.* **28**, 427–434 (2001).
19. M. E. Khosroshahi, M. S. Nourbakhsh, S. Saremi, and F. Tabatabaee, "Characterization of skin tissue soldering using diode laser and ICG: in-vitro studies," *Laser Med. Sci.* **25**, 207–212 (2010).
20. M. E. Khosroshahi, M. S. Nourbakhsh, S. Saremi, A. Hooshyar, S. Rabbani, F. Tabatabai, and M. Sotudeh, "Application of albumin protein and indocyanine green chromophore for tissue soldering using IR diode laser: ex-vivo and in-vivo studies," *Photomed. Laser Surg.* **28**(6), 723–733 (2010).
21. G. Mie, "Contributions to the optics of turbid media, especially colloidal metal solutions," *Ann. Phys.* **25**(3), 377–445 (1908).
22. S. R. Sershen, S. L. Wescott, J. L. West, and N. J. Halas, "An opto-mechanical nanoshell-polymer composite," *Appl. Phys. B* **37**, 379–381 (2001).
23. A. Pinchuk and G. Schatz, "Collective surface plasmon resonance coupling in silver nanoshell arrays," *Appl. Phys. B* **93**(1), 31–38 (2008).

24. T. Brosh, D. Simhon, M. Halpern, A. Ravid, T. Vasilyev, N. Kariv, Z. Nevo, and A. Katzir, "Closure of skin incision in rabbits by laser soldering. II: Tensile strength," *Lasers Surg Med.* **35**, 12–17 (2004).
25. M. Hu, J. Y. Chen, and Z. Y. Li, "Gold nanostructures: engineering their plasmonic properties for biomedical applications," *Chem. Soc. Rev.* **35**, 1084–1094 (2006).
26. Y. Wang, W. Qian, Y. Tan, and S. Ding, "A label-free biosensor based on gold nanoshell monolayers for monitoring biomolecular interactions in diluted whole blood," *Biosens. Bioelectron.* **23**, 1166–1170 (2008).
27. J. B. Jackson, S. L. Westcott, L. R. Hirsch, J. L. West, and N. J. Halas, "Controlling the surface enhanced Raman effect via the nanoshell geometry," *Appl. Phys. Lett.* **82**, 257–259 (2003).
28. A. M. Gobin, M. H. Lee, N. J. Halas, W. D. James, R. A. Drezek, and J. L. West, "Near infrared resonant nanoshells for combined optical imaging and photothermal cancer therapy," *Nano Lett.* **7**(7), 1929–1934 (2007).
29. D. P. O'Neal, L. R. Hirsch, N. J. Halas, J. D. Payne, and J. L. West, "Photo-thermal tumor ablation in mice using near infrared-absorbing nanoparticles," *Cancer Lett.* **209**, 171–176 (2004).
30. J. M. Stern, J. Stanfield, and Y. Lotan, "Efficacy of laser-activated gold nanoshells in ablating prostate cancer cells in vitro," *J. Endourol.* **21**, 939–943 (2007).
31. A. M. Gobin, D. P. O'Neal, D. M. Watkins, N. J. Halas, R. A. Drezek, and J. L. West, "Near infrared laser-tissue welding using nanoshells as an exogenous absorber," *Lasers Surg. Med.* **37**, 123–129 (2005).
32. J. Malicka, I. Gryczynski, C. D. Geddes, and J. R. Lakowicz, "Metal enhanced emission from indocyanine green: A new approach to in vivo imaging," *J. Biomed. Opt.* **8**(3), 472–478 (2003).
33. J. L. Lia, L. Wanga, X. Y. Liua, Z. P. Zhangb, H. C. Guoa, and S. H. Tanga, "In vitro cancer cell imaging and therapy using transferring-conjugated gold nanoparticles," *Cancer Lett.* **274**(2), 319–326 (2009).
34. M. S. Nourbakhsh and M. E. Khosroshahi, "In-vitro studies of skin tissue soldering using gold nanoshells and diode laser," *Lasers Med. Sci.* **26**(1), 49–55 (2011).
35. L. R. Hirsch, R. J. Stafford, J. A. Bankson, S. R. Sershen, B. Rivera, R. E. Price, J. D. Hazle, N. J. Halas, and J. L. West, "Nanoshell-mediated near-infrared thermal therapy of tumors under magnetic resonance guidance," *Proc. Natl. Acad. Sci. U.S.A.* **100**(23), 13549–13554 (2003).
36. R. A. Alvarez-Puebla, D. J. Ross, G. A. Nazri, and R. F. Aroca, "Surface-enhanced Raman scattering on nanoshells with tunable surface plasmon resonance," *Langmuir* **21**, 10504–10508 (2005).
37. M. Gellner, B. Kustner, and S. Schlucker, "Optical properties and SERS efficiency of tunable gold/silver nanoshells," *Vib. Spectrosc.* **50**(1), 43–47 (2009).
38. J. Tang, G. Godlewski, S. Rouy, and G. Delacretaz, "Morphologic changes in collagen fibers after 830 nm diode laser welding," *Lasers Surg. Med.* **2**, 438–443 (1997).
39. K. M. McNally and A. J. Welch, "Laser tissue welding," Chapter 5 of *Biomedical Photonics Handbook*, Chemical Rubber, Boca Raton **39**(1), 39–43 (2003).
40. A. J. Kirsch, C. S. Cooper, J. Gatti, H. C. Scherz, D. A. Canning, S. A. Zderic, and H. M. Snyder, "Laser tissue soldering for hypospadias repair: Results of a controlled prospective clinical trial," *J. Urol.* **65**, 574–577 (2001).
41. M. R. Verdaasdonk, F. C. Holstege, E. D. Jansen, and C. Borst, "Temperature along the surface of modified fiber tips for Nd:YAG laser angioplasty," *Lasers Surg. Med.* **11**, 213–222 (1991).
42. S. D. DeCoste, W. Farinelli, T. Flotte, and R. R. Anderson, "Dye enhanced laser welding for skin closure," *Lasers Surg. Med.* **12**, 25–32 (1992).
43. A. J. Kirsch, J. W. Duckett, H. M. Snyder, D. A. Canning, D. W. Harshaw, P. Howard, E. J. Marcarak, and S. A. Zderic, "Skin flap closure by dermal laser tissue soldering: a wound healing model for sutureless hypospadias repair," *Urology* **50**, 263–272 (1997).
44. L. C. Fung, G. C. Mingin, M. Massicotte, D. Felsen, and D. P. Poppas, "Effects of temperature on tissue thermal injury and wound strength after photothemal wound closure," *Lasers Surg. Med.* **25**, 285–290 (1999).
45. M. Cohen, A. Ravid, V. Scharf, D. Hauben, and A. Katzir, "Temperature controlled burn generation system based on a CO_2 laser and a silver halide fiberoptic radiometer," *Lasers Surg. Med.* **32**, 413–416 (2003).